Cell Reports

Report

hGBP1 Coordinates *Chlamydia* Restriction and Inflammasome Activation through Sequential GTP Hydrolysis

Graphical Abstract

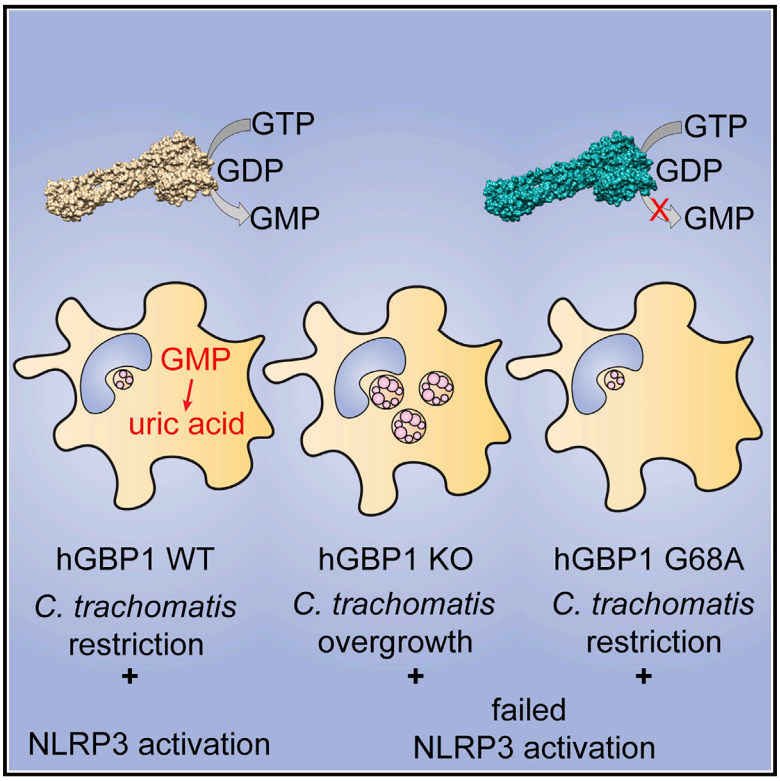

Authors

Audrey Xavier, Munir A. Al-Zeer, Thomas F. Meyer, Oliver Daumke

Correspondence

oliver.daumke@mdc-berlin.de

In Brief

The human guanylate binding protein (hGBP1) is a mechano-chemical GTPase of the dynamin family that hydrolyzes GTP to GMP in two consecutive cleavage steps. Xavier et al. demonstrate that, although GMP production is dispensable for the restriction of *C. trachomatis* growth, it is required for NLRP3 inflammasome activation.

Highlights

- Generation of a hGBP1 mutant with a specific defect in the second hydrolysis step
- GMP production of hGBP1 is dispensable for *Chlamydia* restriction
- GMP production of hGBP1 is required for inflammasome activation
- GMP is metabolized to uric acid that mounts an inflammasome response

Xavier et al., 2020, Cell Reports *31*, 107667
May 19, 2020
https://doi.org/10.1016/j.celrep.2020.107667

CellPress

Cell Reports

CellPress
OPEN ACCESS

Report

hGBP1 Coordinates *Chlamydia* Restriction and Inflammasome Activation through Sequential GTP Hydrolysis

Audrey Xavier,[1,2,3] Munir A. Al-Zeer,[3,4] Thomas F. Meyer,[3] and Oliver Daumke[1,2,5,*]
[1]Crystallography, Max Delbrück Center for Molecular Medicine, Robert-Rössle Str. 10, 13125 Berlin, Germany
[2]Institute for Chemistry and Biochemistry, Freie Universität Berlin, Takustr. 3, 14195 Berlin, Germany
[3]Department of Molecular Biology, Max-Planck Institute for Infection Biology, Charitéplatz 1, 10117 Berlin, Germany
[4]Institute of Biotechnology, TIB 4/3-2, Department of Applied Biochemistry, Technical University of Berlin, Gustav-Meyer-Allee 25, 13355 Berlin, Germany
[5]Lead Contact
*Correspondence: oliver.daumke@mdc-berlin.de
https://doi.org/10.1016/j.celrep.2020.107667

SUMMARY

Human guanylate binding protein 1 (hGBP1) belongs to the dynamin superfamily of GTPases and conveys host defense against intracellular bacteria and parasites. During infection, hGBP1 is recruited to pathogen-containing vacuoles, such as *Chlamydia trachomatis* inclusions, restricts pathogenic growth, and induces the activation of the inflammasome pathway. hGBP1 has a unique catalytic activity to hydrolyze guanosine triphosphate (GTP) to guanosine monophosphate (GMP) in two consecutive cleavage steps. However, the functional significance of this activity in host defense remains elusive. Here, we generate a structure-guided mutant that specifically abrogates GMP production, while maintaining fast cooperative GTP hydrolysis. Complementation experiments in human monocytes/macrophages show that hGBP1-mediated GMP production is dispensable for restricting *Chlamydia trachomatis* growth but is necessary for inflammasome activation. Mechanistically, GMP is catabolized to uric acid, which in turn activates the NLRP3 inflammasome. Our study demonstrates that the unique enzymology of hGBP1 coordinates bacterial growth restriction and inflammasome signaling.

INTRODUCTION

Intracellular bacteria retain a fine balance between survival and detection by the host. The recognition of distinct pathogenic signatures, so-called pathogen-associated molecular patterns (PAMPs), is essential for the host organism to distinguish self from an invading pathogen and to consequently activate an effective immune response (Kim et al., 2016). *Chlamydia trachomatis* (*C. trachomatis*), an obligate intracellular Gram-negative bacterium, is the most common cause of sexually transmitted diseases (Elwell et al., 2016). *C. trachomatis* enters the host cell within a membranous compartment, and in order to avoid detection, it is compelled to reside within this pathogen-containing vacuole (PCV) throughout its life cycle (Kumar and Valdivia, 2009). Thus, *C. trachomatis* infections often remain undetected by the host immune system. How host cells mount immunity against such vacuolar pathogens is poorly understood.

Recently, the interferon-γ (IFN-γ)-induced guanylate binding proteins (GBPs) have emerged as versatile antimicrobial agents of cell-autonomous immunity (Kim et al., 2011). GBPs belong to the dynamin superfamily of large GTPases. Like other dynamin-related proteins, GBPs show nucleotide-dependent oligomerization and fast cooperative GTPase activity (Daumke and Praefcke, 2016; Praefcke and McMahon, 2004). Among the seven hGBPs, hGBP1, hGBP2, and hGBP5 exhibit a C-terminal isoprenylation anchor that enables membrane binding (Britzen-Laurent et al., 2010). These GBPs are recruited to PCVs or the bacterial membrane; it is, therefore, proposed that they engage in a membrane remodeling event that restricts pathogenic growth (Meunier et al., 2014). In turn, the liberation of PAMPs may be sensed by canonical and non-canonical inflammasomes (Meunier et al., 2015; Pilla et al., 2014). The activated inflammasome initiates the secretion of pro-inflammatory cytokines and chemokines that recruit effector immune cells. It also induces inflammatory host cell death, a process termed pyroptosis (Kanneganti, 2015). Accordingly, GBP-deficient cells or mice fail to restrict pathogenic growth and display dampened inflammasome activation (Degrandi et al., 2013; Finethy et al., 2015; Fisch et al., 2019; Pilla et al., 2014). How GBPs coordinate these two processes and the exact role of GBPs in inflammasome activation have not been addressed so far.

hGBP1 has a unique catalytic property of hydrolyzing guanosine triphosphate (GTP) to guanosine monophosphate (GMP) in two consecutive cleavage reactions (Praefcke et al., 1999; Schwemmle and Staeheli, 1994). Crystal structures of the hGBP1 GTPase domain (G-domain) reveal that the ribose

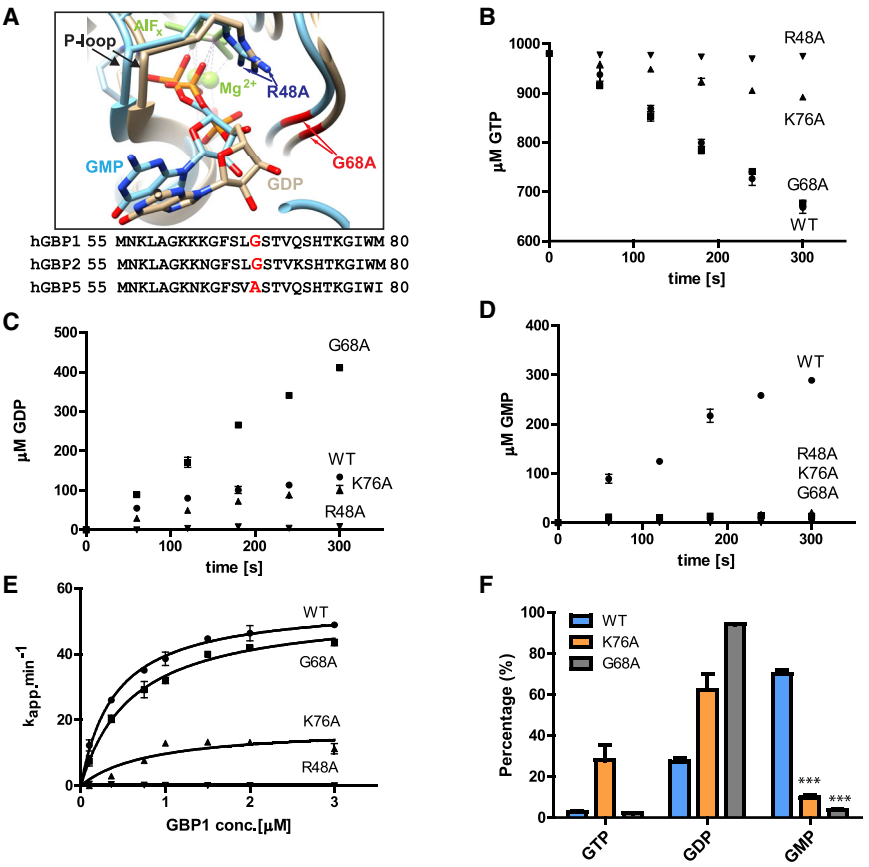

Figure 1. The hGBP1 G68A Mutant Exhibits an Impaired Consecutive Hydrolysis Step

(A) (Top) Superimposition of hGBP1 G-domain structures bound to GDP·AlF_x (brown; PDB: 2b92) and GMP·AlF_x (blue; PDB: 2b8w). (Bottom) Sequence alignment of human GBP1, GBP2, and GBP5. Position 68 is marked in red.

(B–D) GTP hydrolysis (B), GDP production (C), and GMP production (D) of 2 µM hGBP1 WT (●), G68A (■), K76A (▲), or R48A (▼) were followed by an high-performance liquid chromatography (HPLC)-based approach. Data represent the average of two independent measurements ± range. Error bars smaller than the data points are not indicated.

(E) Cooperative GTP hydrolysis rate of indicated hGBP1 proteins obtained by plotting specific activity against protein concentration. Data represent the average of two independent measurements ± range. Error bars smaller than the data points are not indicated.

(F) End product formation of GTP hydrolysis after reacting with 2 µM of indicated hGBP1 proteins for 30 min; n = 3. Error bars indicate the standard error of the mean (SEM). *p < 0.05, **p < 0.01, ***p < 0.001, two-way ANOVA.

backbone of the nucleotide moiety is pushed forward upon GTP hydrolysis. As a result, the β-phosphate occupies the position, which was previously occupied by the γ-phosphate. Thus, GDP can be cleaved to GMP with the same catalytic machinery (Ghosh et al., 2006). However, the functional significance of its distinctive enzymatic property remains unknown.

To decipher this enzymatic function, we generated a structure-guided hGBP1 mutant that maintains GTP hydrolysis but specifically abolishes the second step of the hydrolysis reaction. Using a gene knockout (KO) system and reconstitution experiments on human monocytes, we show that the second hydrolysis step is dispensable for bacterial restriction but is necessary for mounting inflammasome activation.

RESULTS

The hGBP1 G68A Mutant Retains Fast, Cooperative GTP Hydrolysis While Displaying Reduced GMP Production

Because the two-step cleavage mechanism of GTP to GMP by hGBP1 requires the movement of the ribose backbone of the cleaved GDP moiety, a point mutation in the G-domain of hGBP1 was designed to sterically lock GDP in the nucleotide binding site and, thus, prevent the second hydrolysis step (Figure 1A). Several glycine residues surround GTP in the catalytic site and provide the necessary peptide backbone flexibility that enables nucleotide relocation. Among these glycines, we focused on Gly68 for two reasons. First, in the reported crystal structure (*Ghosh et al., 2006*), Gly68 is in close proximity to the ribose moiety of GDP during GTP hydrolysis, and its mutation into a bulkier amino acid may consequently interfere with nucleotide displacement. Second, we compared hGBP1 to hGBP5, which can cleave GTP only to GDP (Neun et al., 1996; Wehner and Herrmann, 2010). According to the sequence alignment, Gly68 is substituted with alanine in hGBP5 (Figure 1A).

The G68A mutant of hGBP1 retained a similar GTP hydrolysis rate to that of the wild-type (WT) protein (Figure 1B). However, the G68A mutation completely abolished GMP production (Figures 1C, 1D, and 1F). Mutations in Lys76 or His74 in the conserved switch I region of the G-domain have been previously shown to abrogate GMP production (Praefcke et al., 2004). Nonetheless, unlike G68A, the K76A mutation led to a general reduction in GTP hydrolysis (Figure 1B). Mutating Arg48, which stabilizes the transition state of GTP hydrolysis, to alanine completely abolished GTP hydrolysis (Figures 1B–1E), which is also consistent with previous data (Praefcke et al., 2004).

To further compare the specific catalytic activities of the mutants, we performed a detailed time- and concentration-dependent enzymatic characterization. In comparison to the WT protein, we show that the dimerization-dependent GTP hydrolysis activity of the G68A mutant was not impaired. Although the K76A mutation retained cooperativity, this mutation led to a 4-fold decrease in the maximal GTP hydrolysis activity (Figure 1E). Collectively, among the tested hGBP1 mutants that abolish GMP production, the G68A mutant had the most WT-comparable GTP hydrolysis activity, and we therefore utilized this mutant for the subsequent functional studies.

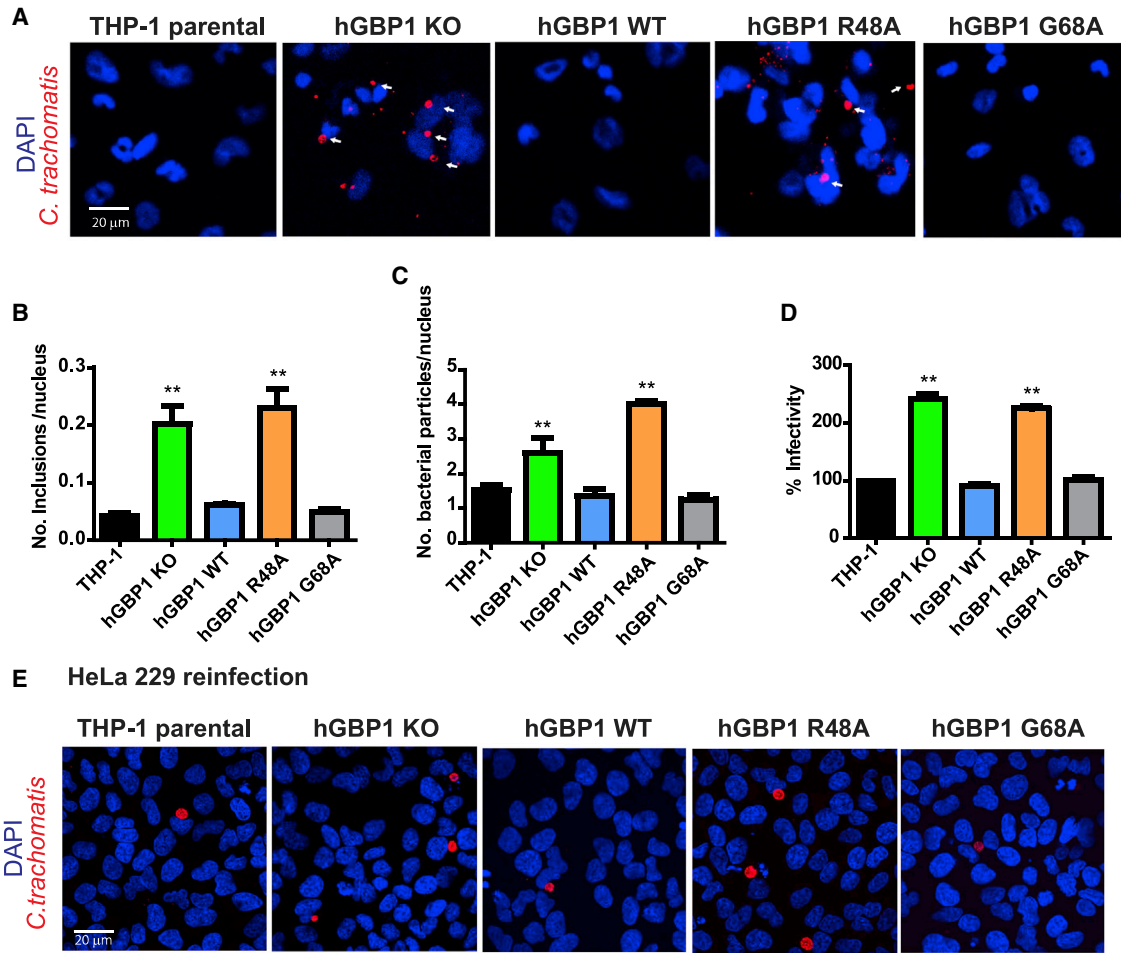

Figure 2. hGBP1 G68A Mutant Is Able to Restrict *C. trachomatis*

(A) Representative images of indicated THP-1 cell lines infected with *C. trachomatis* at MOI of 5 for 24 h. White arrows indicate inclusions. Red, *C. trachomatis*. Blue, 4′,6-diamidino-2-phenylindole (DAPI). Scale bars, 20 μm.

(B and C) *C. trachomatis* inclusions larger (B) or smaller (C) than the size of 2-μm diameter were quantified by scanning the nuclei (30–40 per image) of all the cells, as indicated in (A) (n = 3).

(D) Influence of hGBP1 mutants on *C. trachomatis* infectious progeny. *C. trachomatis* inclusions were isolated from the infected various THP-1 cells; the infectivity was determined by the re-infection of HeLa 229 cells, normalized to the parental THP-1 cells.

(E) Representative images of (D). Red, *C. trachomatis.* Blue, DAPI.

All error bars indicate SEM. *$p < 0.05$, **$p < 0.01$, one-way ANOVA. See also Figure S1.

Consecutive GTP Hydrolysis Is Dispensable for the Restriction of *C. trachomatis*

To characterize the role of the second-step GDP hydrolysis for pathogen restriction, we knocked out hGBP1 in THP-1 cells, a human monocyte cell line, by using CRISPR-Cas9 technology. We then reconstituted the KO cells with lentivirus-expressed WT hGBP1, the hGBP1 mutants, R48A or G68A, or GFP as a negative control. The depletion of endogenous hGBP1 and the expression of exogenous constructs were confirmed by western blot (Figure S1A).

Parental THP-1 cells and the newly generated cell lines were infected with *C. trachomatis*, followed by immunostaining against major outer membrane protein (MOMP), an antigen of *C. trachomatis*. In agreement with a previous study, hGBP1 KO cells presented an increased number and size of *C. trachomatis* inclusions (Figures 2A–2C) (Al-Zeer et al., 2013). Re-expression of WT hGBP1, but not the R48A mutant, reduced *C. trachomatis* inclusions, indicating that hGBP1-mediated GTP hydrolysis is vital for *C. trachomatis* restriction. Surprisingly, G68A mutants restricted *C. trachomatis* comparably to WT hGBP1-expressing cells (Figures 2A–2C).

To further substantiate these findings, we tested the requirement of consecutive GTP hydrolysis for restricting infectious *C. trachomatis* progeny by conducting a re-infection assay in HeLa cells. hGBP1 KO cells and R48A mutants increased the production of *C. trachomatis* elementary bodies, whereas WT hGBP1-expressing cells and G68A mutants significantly reduced their production (Figures 2D and 2E). Thus, consecutive GTP hydrolysis is dispensable for hGBP1-mediated *Chlamydia* restriction.

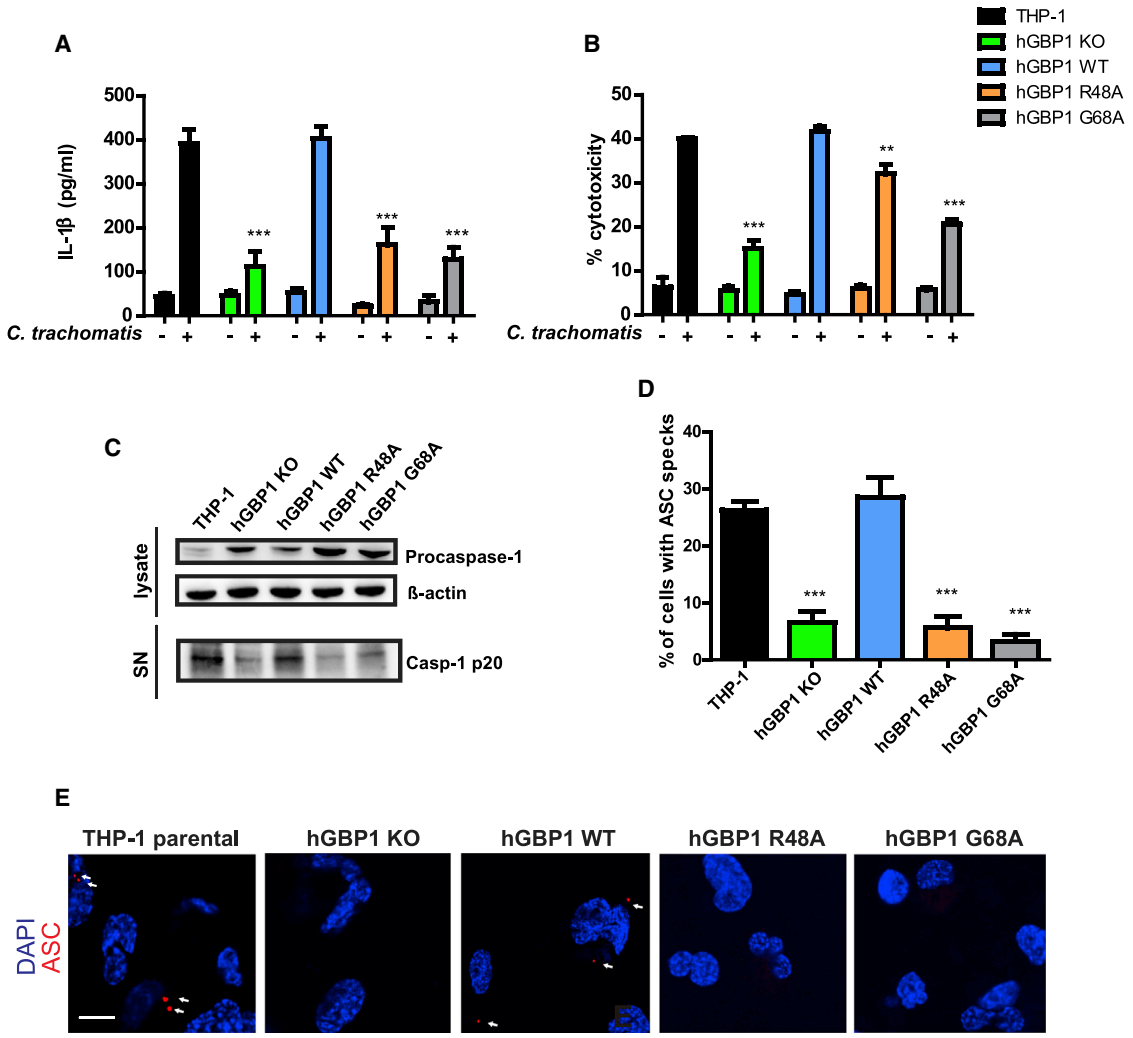

Figure 3. The Consecutive Hydrolysis of hGBP1 Is Required for Inflammasome Activation

(A) Inflammasome activation was examined by IL-1β ELISA. Cell lines were infected with *C. trachomatis* at MOI of 30 for 24 h; n = 3; two-way ANOVA.

(B) Cell death was measured by measuring the release of lactate dehydrogenase in LPS + IFN-γ-stimulated THP-1 cells infected with *C. trachomatis* at an MOI of 30 for 24 h; n = 3; two-way ANOVA.

(C) Inflammasome activation was examined by immunoblotting against caspase-1. Cell lines were infected with *C. trachomatis* at an MOI of 30 for 24 h. The blot is a representative result of two independent experiments.

(D) Quantification of inflammasome ASC specks of indicated cell lines infected with *C. trachomatis* at an MOI of 30 for 24 h; n = 3; one-way ANOVA.

(E) Representative images of (D). Red, ASC specks. Blue, DAPI. Scale bar, 10 μm.

All error bars indicated SEM. *p < 0.05, **p < 0.01, ***p < 0.001. See also Figure S2.

Consecutive GTP Hydrolysis Is Required for Inflammasome Activation

It has been previously demonstrated that GBPs are required for inflammasome activation (Fisch et al., 2019; Man et al., 2015; Meunier et al., 2014, 2015; Pilla et al., 2014). Inflammasome activation leads to Gasdermin D-mediated cell death (pyroptosis), caspase-1-dependent processing, and the secretion of interleukin-1β (IL-1β). We evaluated the cell death rate of *C. trachomatis*-infected THP-1 cells by measuring lactate dehydrogenase (LDH) release and IL-1β secretion. As expected, KO cells showed a significant reduction in IL-1β secretion and cell death rate compared with the parental cells (Figures 3A and 3B). These defects were rescued by re-expression of hGBP1 WT. In contrast, expression of the R48A mutant failed to rescue IL-1β secretion (Figure 3A), concomitantly with unexpected increased cell death (Figure 3B). Screening of inhibitors that target various cell death mechanisms showed that R48A mutants died due to necroptosis (Figure S1B). The surprising link between the hGBP1 R48A mutation and the induction of necroptosis needs further investigation.

Interestingly, the G68A mutant failed to secrete IL-1β and induce cell death in an infection-dependent manner, which was comparable with KO cells (Figures 3A and 3B). We also examined the status of caspase-1 activation by western blotting

of cell culture supernatants. In contrast to hGBP1 WT the G68A mutant did not rescue the secretion of mature caspase-1 subunit p20 in hGBP1 KO cells (Figure 3C). We reasoned that the reduced secretion of caspase-1 and inflammatory cytokines are the results of impaired inflammasome activation.

A previous study demonstrates that hGBP2 can also hydrolyze GTP to GMP but much less efficiently than hGBP1 (~10% of hGBP1) (Neun et al., 1996). Depletion of hGBP2 in THP-1 cells led to a non-significant marginal reduction of IL-1β release and cell death (Figure S1C), despite an efficient knockdown (Figure S1D). Thus, activation of the inflammasome is not a general feature of all hGBPs. Instead, it may be related to the exceptionally high GMP production by hGBP1.

hGBP1 Activates the NLRP3 Inflammasome

hGBPs have been shown to activate the canonical nucleotide-binding oligomerization domain (NOD-), leucine-rich repeat (LRR-), and pyrin domain-containing protein 3 (NLRP3) inflammasome either directly or indirectly through the non-canonical caspase-4-mediated pathway (Meunier et al., 2014; Pilla et al., 2014). To prove whether consecutive GTP hydrolysis is required for inflammasome activation, we first infected hGBP1 KO cells that re-express hGBP1 WT or the R48A or G68A mutant with *C. trachomatis*. We then examined infection-dependent NLRP3 activation by monitoring the speck formation of the inflammasome adaptor ASC (apoptosis-associated Speck-like protein containing a caspase activation and recruitment domain). In line with the previous experiments, G68A mutants formed fewer ASC specks compared with hGBP1 WT-expressing cells (Figures 3D and 3E). To verify that NLRP3 is the major inflammasome pathway induced by *C. trachomatis* infection, we treated the cells with the NLPR3 inhibitor MCC950. MCC950 treatment largely abolished infection-induced IL-1β secretion and pyroptosis (Figure S2A). The effect of MCC950 was also confirmed in a culture of human primary macrophages (Figure S2B).

Next, we asked whether caspase-4 activation causes NLRP3 inflammasome activation. Transient knockdown of caspase-4 inhibited IL-1β release and cell death in response to intracellular lipopolysaccharide (LPS), a well-established activator of caspase-4 (Figure S2C) (Shi et al., 2014). In contrast, caspase-4 knockdown had no effect on IL-1β secretion and pyroptosis following *C. trachomatis* infection (Figure S2C). Taken together, these results suggest that hGBP1-mediated consecutive hydrolysis of GTP to GMP is required for the canonical caspase-4-independent activation of the NLRP3 inflammasome.

Uric Acid (UA) Synthesis Is Required for Inflammasome Activation upon *Chlamydia* Infection

We next investigated the potential mechanism by which hGBP1 promotes NLRP3 inflammasome activation. Several intracellular danger patterns are known to activate the NLRP3 inflammasome, among which UA is one (Braga et al., 2017; Kimball et al., 2019; Martinon et al., 2006). Interestingly, GMP can be catabolized to UA through three enzymatic steps (Figure 4A). We, thus, reasoned that hGBP1 oligomerization on the vacuolar membrane would result in a local rise in GMP concentration. Subsequently, this could favor catabolism to UA, which in turn would activate the NLRP3 inflammasome.

An essential prediction of our model is that enzymes involved in the metabolism of GMP to UA would be localized to the PCV or regulated during infection. Indeed, as *Chlamydia* are obligate intracellular pathogens, many metabolites and metabolic enzymes are known to be hijacked from the host system and recruited to the inclusion membrane (Saka and Valdivia, 2010). We examined the localization of xanthine oxidase, a key enzyme involved in the last step of xanthine oxidization to UA. In uninfected cells, xanthine oxidase was evenly distributed throughout the cell. In contrast, this enzyme displayed a marked vesicular pattern in infected cells, which strongly co-localized with the inclusions (Figure S3A). Furthermore, based on our microarray data from a previous study, we observed that the transcripts of guanine deaminase (GDA), which catalyzes the upstream step of xanthine oxidase, are significantly increased upon *C. trachomatis* infection (Mehlitz et al., 2010). qRT-PCR of GDA validated these microarray results (Figure S3B).

Next, we asked if blocking UA synthesis can impair inflammasome activation in response to *C. trachomatis* infection. First, we used allopurinol, a clinically approved xanthine oxidase inhibitor used for gout medication. Remarkably, co-treatment of cells with allopurinol mitigated *C. trachomatis*-induced pyroptosis and ASC speck formation in a concentration-dependent manner (Figures 4B and S3C). Accordingly, we detected a sharp reduction of IL-1β secretion in the cell supernatant (Figure 4B), whereas IL-1β expression was not affected at the mRNA level (Figure S3D). Allopurinol blocked inflammasome activation in human primary macrophages as well (Figure S3F). Importantly, the effect of allopurinol was specific to *C. trachomatis* infection because it had no effect on other inflammasome activators, such as poly (dA:dT), flagellin, and LPS/ATP (Figures S3E and S3F). As a second approach, we genetically inactivated the metabolic pathway of UA production. To this end, we transiently knocked down the enzyme GDA due to its specific involvement in GMP catabolism rather than that of AMP. The efficient downregulation of GDA after small interfering RNA (siRNA) transfection was validated by qRT-PCR (Figure S4A). Compared with control scrambled siRNA, all three GDA siRNAs significantly inhibited cell death and increased ASC speck formation and IL-1β secretion upon infection with *C. trachomatis* (Figures 4C and S4B); IL-1β mRNA expression was unaffected (Figure S4C). Notably, GDA knockdown did not reduce bacterial growth, indicating that the impaired inflammasome activation is not an indirect effect of a lower bacterial load (Figure S4D).

hGBP1-Produced GMP Is Metabolized to UA

To verify our hypothesis, we measured UA concentrations upon *C. trachomatis* infection in THP-1 cells. We observed an infection-dependent increase of UA in parental cells as well as of hGBP1 WT-expressing cells, whereas hGBP1 KO cells, R48A mutants, and G68A mutants showed no induction of UA (Figure 4D). Next, we applied an antibody against UA, which was originally generated for the diagnostics of rheumatic arthritis. We observed a strong UA immunostaining around early *C. trachomatis* vacuoles as well as around mature inclusions that spread throughout the cytoplasm (Figure S4E). UA staining was abolished in allopurinol-treated cells, confirming the

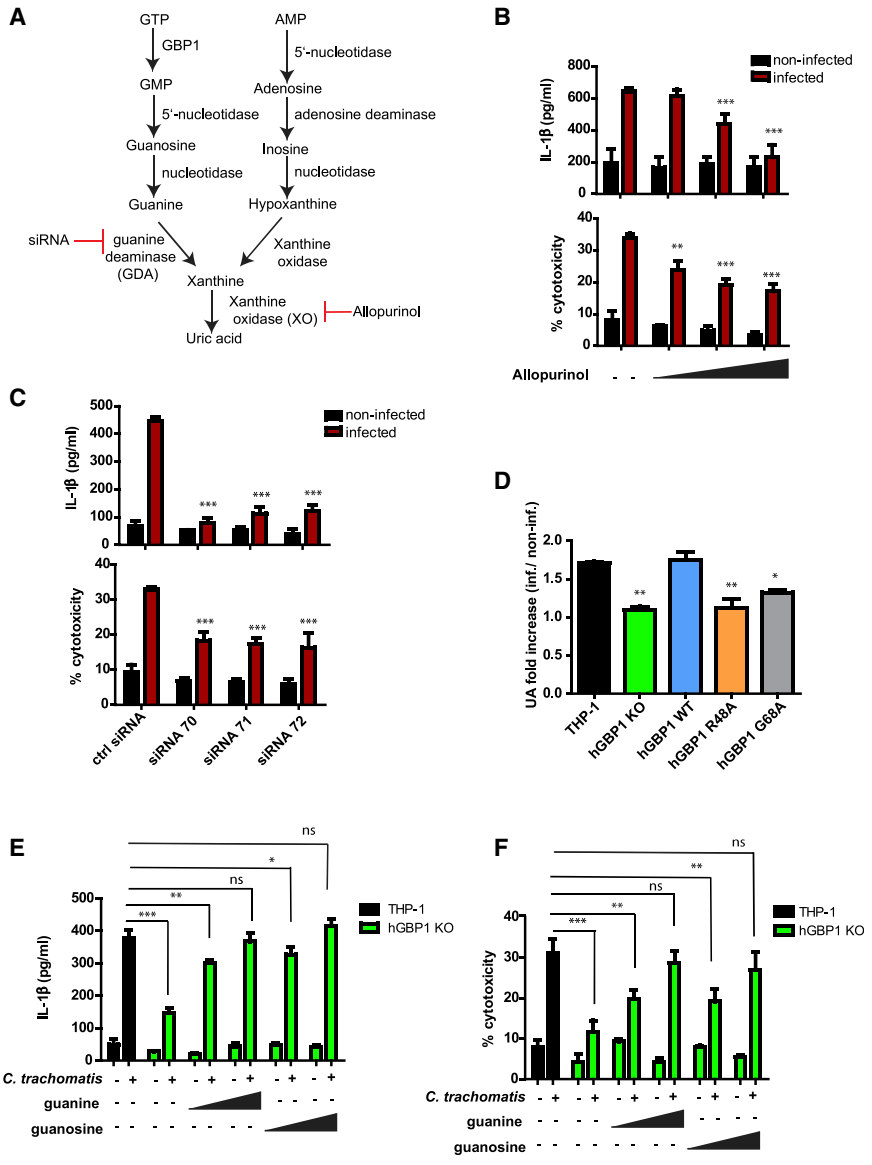

Figure 4. hGBP1 Mediates Inflammasome Activation by Uric Acid

(A) Metabolic pathway of GMP degradation to uric acid. The enzyme GDA was knocked down by siRNA, and the enzyme xanthine oxidase was inhibited with the chemical compound allopurinol.

(B and C) LDH release and IL-1β ELISA of THP-1 cells treated with increasing concentrations of allopurinol (50, 100, and 500 μM) (B) or transfected with control or three different siRNAs against GDA (C). The cells were stimulated with IFNγ + LPS and infected with *C. trachomatis* at an MOI of 30 for 24 h; n = 3; two-way ANOVA.

(D) Fold change of UA concentrations in the cell culture supernatants of infected THP-1 cells versus non-infected THP-1 cells. The cells were stimulated with IFN-γ + LPS and infected with *C. trachomatis* at an MOI of 30 for 24 h; n = 3; one-way ANOVA.

(E and F) IL-1β ELISA and LDH release of hGBP1 KO THP-1 cells, which were infected with *C. trachomatis* at an MOI of 30 for 24 h and treated with increasing concentrations of guanine or guanosine (0.5 mM and 1 mM); n = 3; statistical significance was determined in comparison to the parental cell line by two-way ANOVA.

All error bars indicate SEM. *p < 0.05, **p < 0.01, ***p < 0.001. See also Figures S3 and S4.

specificity of the antibody (Figure S4E). UA has been associated with NLRP3 activation by triggering mitochondrial reactive oxygen species (ROS) production (Braga et al., 2017). Consistently, we observed an increase of mitochondrial ROS in *C. trachomatis*-infected cells, which was abolished thereof by allopurinol treatment (Figure S4F). Lastly, we asked whether infection-induced inflammasome activation could be rescued in hGBP1 KO cells and G68A mutants by feeding back intermediate metabolites of UA catabolism (Figure 4A). Remarkably, the addition of guanine and guanosine to hGBP1 KO cells and G68A mutant cells led to a dose-dependent increase of IL-1β secretion and pyroptosis (Figures 4E, 4F, S4G, and S4H).

In summary, we propose that hGBP1-mediated inflammasome activation occurs through consecutive cleavage of GTP to GMP, leading to local accumulation of UA, consequently activating the NLRP3 inflammasome.

DISCUSSION

In this study, we generated a specific catalytic mutant of hGBP1 that retains cooperative GTP hydrolysis (i.e., at a comparable rate to the WT protein), while being impaired in the consecutive hydrolysis step. By using this mutant, we explored hGBP1's unique function in GMP production by using an infection model with the obligate intracellular pathogen *C. trachomatis*. hGBP1 has been implicated in restricting pathogenic growth and mediating inflammasome activation. Here, we show that the GTPase activity of hGBP1 tightly coordinates these two functions. Thus, similar to other dynamin-related proteins, recruitment of hGBP1 to the PCV is thought to activate GTP hydrolysis, which may be linked to membrane remodeling and the destruction of the PCV (Daumke and Praefcke, 2016; Meunier et al., 2014). We demonstrate that GMP, produced in the succeeding second nucleotide cleavage step, then serves as a precursor of UA. In this scenario, the PCV acts as a platform that mediates the recruitment of hGBP1 and xanthine oxidase to the *C. trachomatis* inclusions to initiate inflammasome signaling.

At the same time, *C. trachomatis* infection led to an increase in GDA expression (Figure S1C). Thus far, it has been unclear whether this regulation of nucleotide metabolizing enzymes is merely part of a host defense mechanism or a way of *C. trachomatis* to redirect the host metabolism as part of a survival strategy. Downregulation of GDA did not affect pathogenic

growth, suggesting that GDA activity and UA formation are not required for the survival of *C. trachomatis* under regular conditions. However, the loss of hGBP1-mediated GMP production reduced *C. trachomatis*-induced cell death, implying a direct link between guanine catabolism and inflammasome activation. Although we ruled out the contribution of hGBP2 to *C. trachomatis*-dependent UA formation, we cannot exclude the possibility for other hGBPs that can execute this second hydrolysis step.

Mouse macrophages use multiple inflammasome pathways in response to *C. trachomatis* infection (Finethy et al., 2015). Conversely, our study indicates that the UA-NLRP3 axis is mainly responsible for the host response to *C. trachomatis* infections in humans. Furthermore, our data suggest that inflammasome activation in human macrophages is rather independent of PAMP liberation by hGBPs, substantiating the finding that inflammation occurs over a unified pathway. Therefore, we propose that allopurinol could be a potential therapeutic application for reducing acute inflammation in patients suffering from *C. trachomatis* infection. In the future, it might be useful to test whether inflammasome activation is triggered by the same pathway in response to other obligate intracellular pathogens.

STAR★METHODS

Detailed methods are provided in the online version of this paper and include the following:

- KEY RESOURCES TABLE
- RESOURCE AVAILABILITY
  - Lead Contact
  - Materials Availability
  - Data and Code Availability
- EXPERIMENTAL MODEL AND SUBJECT DETAILS
  - Cell Lines
  - Human Primary Macrophages
  - Microbe strain and culture
- METHOD DETAILS
  - Expression constructs
  - Protein preparation
  - GTP hydrolysis assay
  - Cell culture treatments and C. trachomatis infection
  - CRISPR Cas9 mediated Knock out of hGBP1 in THP-1
  - Immunostaining and ASC speck count
  - Inclusion count
  - Infectivity assay
  - LDH cytotoxicity assay
  - ELISA
  - mtROS measurement
  - Uric acid measurement
- QUANTIFICATION AND STATISTICAL ANALYSIS
  - Image Analysis
  - Cell Biological Assays

SUPPLEMENTAL INFORMATION

Supplemental Information can be found online at https://doi.org/10.1016/j.celrep.2020.107667.

ACKNOWLEDGMENTS

We thank Jörg Angermann and Kfir Lapid (Max-Planck Institute for Infection Biology) for expert technical assistance and editorial assistance, respectively. We thank Dominik Müller and Sabrina Geisberger (Experimental and Clinical Research Center from MDC and Charité) for providing us with human-primary-monocyte-derived macrophages. This work was carried out in part on the premises of MPI for Infection Biology and funded by grants of the Helmholtz Society Future Topic "Immunology and Inflammation," Germany (ZT-0027 to O.D.) and the Deutsche Forschungsgemeinschaft, Germany (SFB 958 and A12 to O.D.).

AUTHOR CONTRIBUTIONS

A.X. conceived the project, performed the experiments, analyzed the data, and wrote the manuscript. M.A.A.-Z. initially taught A.X. how to perform chlamydia infection and related assays. T.F.M. and O.D. supervised the work and wrote and edited the manuscript.

DECLARATION OF INTERESTS

We declare no conflict of interest.

Received: October 16, 2019
Revised: March 18, 2020
Accepted: April 28, 2020
Published: May 19, 2020

REFERENCES

Al-Zeer, M.A., Al-Younes, H.M., Braun, P.R., Zerrahn, J., and Meyer, T.F. (2009). IFN-γ-inducible Irga6 mediates host resistance against Chlamydia trachomatis via autophagy. PLoS One *4*, e4588.

Al-Zeer, M.A., Al-Younes, H.M., Lauster, D., Abu Lubad, M., and Meyer, T.F. (2013). Autophagy restricts Chlamydia trachomatis growth in human macrophages via IFNG-inducible guanylate binding proteins. Autophagy *9*, 50–62.

Braga, T.T., Forni, M.F., Correa-Costa, M., Ramos, R.N., Barbuto, J.A., Branco, P., Castoldi, A., Hiyane, M.I., Davanso, M.R., Latz, E., et al. (2017). Soluble Uric Acid Activates the NLRP3 Inflammasome. Sci. Rep. *7*, 39884.

Britzen-Laurent, N., Bauer, M., Berton, V., Fischer, N., Syguda, A., Reipschläger, S., Naschberger, E., Herrmann, C., and Stürzl, M. (2010). Intracellular trafficking of guanylate-binding proteins is regulated by heterodimerization in a hierarchical manner. PLoS One *5*, e14246.

Campeau, E., Ruhl, V.E., Rodier, F., Smith, C.L., Rahmberg, B.L., Fuss, J.O., Campisi, J., Yaswen, P., Cooper, P.K., and Kaufman, P.D. (2009). A versatile viral system for expression and depletion of proteins in mammalian cells. PLoS One *4*, e6529.

Daumke, O., and Praefcke, G.J. (2016). Invited review: Mechanisms of GTP hydrolysis and conformational transitions in the dynamin superfamily. Biopolymers *105*, 580–593.

Degrandi, D., Kravets, E., Konermann, C., Beuter-Gunia, C., Klümpers, V., Lahme, S., Wischmann, E., Mausberg, A.K., Beer-Hammer, S., and Pfeffer, K. (2013). Murine guanylate binding protein 2 (mGBP2) controls Toxoplasma gondii replication. Proc. Natl. Acad. Sci. USA *110*, 294–299.

Elwell, C., Mirrashidi, K., and Engel, J. (2016). Chlamydia cell biology and pathogenesis. Nat. Rev. Microbiol. *14*, 385–400.

Finethy, R., Jorgensen, I., Haldar, A.K., de Zoete, M.R., Strowig, T., Flavell, R.A., Yamamoto, M., Nagarajan, U.M., Miao, E.A., and Coers, J. (2015). Guanylate binding proteins enable rapid activation of canonical and noncanonical inflammasomes in Chlamydia-infected macrophages. Infect. Immun. *83*, 4740–4749.

Fisch, D., Bando, H., Clough, B., Hornung, V., Yamamoto, M., Shenoy, A.R., and Frickel, E.-M. (2019). Human GBP1 is a microbe-specific gatekeeper of macrophage apoptosis and pyroptosis. EMBO J. *38*, e100926.

Ghosh, A., Praefcke, G.J.K., Renault, L., Wittinghofer, A., and Herrmann, C. (2006). How guanylate-binding proteins achieve assembly-stimulated processive cleavage of GTP to GMP. Nature *440*, 101–104.

Kanneganti, T.-D. (2015). The inflammasome: firing up innate immunity. Immunol. Rev. *265*, 1–5.

Kim, B.-H., Shenoy, A.R., Kumar, P., Das, R., Tiwari, S., and MacMicking, J.D. (2011). A family of IFN-γ-inducible 65-kD GTPases protects against bacterial infection. Science *332*, 717–721.

Kim, B.-H., Chee, J.D., Bradfield, C.J., Park, E.-S., Kumar, P., and MacMicking, J.D. (2016). Interferon-induced guanylate-binding proteins in inflammasome activation and host defense. Nat. Immunol. *17*, 481–489.

Kimball, A.S., Davis, F.M., denDekker, A., Joshi, A.D., Schaller, M.A., Bermick, J., Xing, X., Burant, C.F., Obi, A.T., Nysz, D., et al. (2019). The Histone Methyltransferase Setdb2 Modulates Macrophage Phenotype and Uric Acid Production in Diabetic Wound Repair. Immunity *51*, 258–271.e5.

Kumar, Y., and Valdivia, R.H. (2009). Leading a sheltered life: intracellular pathogens and maintenance of vacuolar compartments. Cell Host Microbe *5*, 593–601.

Man, S.M., Karki, R., Malireddi, R.K.S., Neale, G., Vogel, P., Yamamoto, M., Lamkanfi, M., and Kanneganti, T.-D. (2015). The transcription factor IRF1 and guanylate-binding proteins target activation of the AIM2 inflammasome by Francisella infection. Nat. Immunol. *16*, 467–475.

Martinon, F., Pétrilli, V., Mayor, A., Tardivel, A., and Tschopp, J. (2006). Gout-associated uric acid crystals activate the NALP3 inflammasome. Nature *440*, 237–241.

Mehlitz, A., Banhart, S., Mäurer, A.P., Kaushansky, A., Gordus, A.G., Zielecki, J., Macbeath, G., and Meyer, T.F. (2010). Tarp regulates early Chlamydia-induced host cell survival through interactions with the human adaptor protein SHC1. J. Cell Biol. *190*, 143–157.

Meunier, E., Dick, M.S., Dreier, R.F., Schürmann, N., Kenzelmann Broz, D., Warming, S., Roose-Girma, M., Bumann, D., Kayagaki, N., Takeda, K., et al. (2014). Caspase-11 activation requires lysis of pathogen-containing vacuoles by IFN-induced GTPases. Nature *509*, 366–370.

Meunier, E., Wallet, P., Dreier, R.F., Costanzo, S., Anton, L., Rühl, S., Dussurgey, S., Dick, M.S., Kistner, A., Rigard, M., et al. (2015). Guanylate-binding proteins promote activation of the AIM2 inflammasome during infection with Francisella novicida. Nat. Immunol. *16*, 476–484.

Neun, R., Richter, M.F., Staeheli, P., and Schwemmle, M. (1996). GTPase properties of the interferon-induced human guanylate-binding protein 2. FEBS Lett. *390*, 69–72.

Pettersen, E.F., Goddard, T.D., Huang, C.C., Couch, G.S., Greenblatt, D.M., Meng, E.C., and Ferrin, T.E. (2004). UCSF Chimera–a visualization system for exploratory research and analysis. J. Comput. Chem. *25*, 1605–1612.

Pilla, D.M., Hagar, J.A., Haldar, A.K., Mason, A.K., Degrandi, D., Pfeffer, K., Ernst, R.K., Yamamoto, M., Miao, E.A., and Coers, J. (2014). Guanylate binding proteins promote caspase-11-dependent pyroptosis in response to cytoplasmic LPS. Proc. Natl. Acad. Sci. USA *111*, 6046–6051.

Praefcke, G.J., and McMahon, H.T. (2004). The dynamin superfamily: universal membrane tubulation and fission molecules? Nat. Rev. Mol. Cell Biol. *5*, 133–147.

Praefcke, G.J.K., Geyer, M., Schwemmle, M., Kalbitzer, H.R., and Herrmann, C. (1999). Nucleotide-binding characteristics of human guanylate-binding protein 1 (hGBP1) and identification of the third GTP-binding motif. J. Mol. Biol. *292*, 321–332.

Praefcke, G.J.K., Kloep, S., Benscheid, U., Lilie, H., Prakash, B., and Herrmann, C. (2004). Identification of residues in the human guanylate-binding protein 1 critical for nucleotide binding and cooperative GTP hydrolysis. J. Mol. Biol. *344*, 257–269.

Saka, H.A., and Valdivia, R.H. (2010). Acquisition of nutrients by Chlamydiae: unique challenges of living in an intracellular compartment. Curr. Opin. Microbiol. *13*, 4–10.

Sanjana, N.E., Shalem, O., and Zhang, F. (2014). Improved vectors and genome-wide libraries for CRISPR screening. Nat. Methods *11*, 783–784.

Schneider, C.A., Rasband, W.S., and Eliceiri, K.W. (2012). NIH Image to ImageJ: 25 years of image analysis. Nat. Methods *9*, 671–675.

Schwemmle, M., and Staeheli, P. (1994). The interferon-induced 67-kDa guanylate-binding protein (hGBP1) is a GTPase that converts GTP to GMP. J. Biol. Chem. *269*, 11299–11305.

Shi, J., Zhao, Y., Wang, Y., Gao, W., Ding, J., Li, P., Hu, L., and Shao, F. (2014). Inflammatory caspases are innate immune receptors for intracellular LPS. Nature *514*, 187–192.

Wang, X., and Seed, B. (2003). A PCR primer bank for quantitative gene expression analysis. Nucleic Acids Res. *31*, e154.

Wehner, M., and Herrmann, C. (2010). Biochemical properties of the human guanylate binding protein 5 and a tumor-specific truncated splice variant. FEBS J. *277*, 1597–1605.

STAR★METHODS

KEY RESOURCES TABLE

REAGENT or RESOURCE	SOURCE	IDENTIFIER
Antibodies		
Rat monoclonal anti hGBP1	Santa Cruz Biotechnology	Cat#sc-53857; RRID:AB_2109333
Goat polyclonal anti-MOMP	Bio-Rad (formerly AbD serotec)	Cat#1990-0804; RRID:AB_620522
Rabbit polyclonal anti-Caspase-1	Cell Signaling Technology	Cat#2225S; RRID:AB_2243894
Rabbit polyclonal anti-Caspase-4	Cell Signaling Technology	Cat# 4450; RRID:AB_1950386
Rabbit polyclonal anti-ASC	Proteintech	Cat# 10500-1-AP; RRID:AB_2174862
Mouse monoclonal anti-Xanthine Oxidase	Santa Cruz Biotechnology	Cat#sc-398548
Rabbit polyclonal anti UA	Abcam	Cat# ab53000; RRID:AB_883382
Bacterial and Virus Strains		
lentiCRISPR v2	Sanjana et al., 2014	Addgene #52961
plenti CMV GFP Hygro	Campeau et al., 2009	Addgene # 17446
lentiCRISPR v2-hGBP1-KO	This paper	N/A
Plenti CMV GFP Hygro hGBP1 WT	This paper	N/A
Plenti CMV GFP Hygro hGBP1 R48A	This paper	N/A
Plenti CMV GFP Hygro hGBP1 G68A	This paper	N/A
C. trachomatis, serovar L2	ATCC	VR-902B
Chemicals, Peptides, and Recombinant Proteins		
Phorbol 12-Myristate 13-Acetate	Sigma-Aldrich	Cat# 524400, CAS 16561-29-8
Human recombinant IFN-γ	Merck Millipore	Cat# IF002
Human recombinant M-CSF	Sigma	Cat# M6518
LPS, E. Coli O111:B4	Merck Millipore	Cat# LPS25
Flagellin	AdipoGen	Cat#AG-40B-0025-C010
Poly (dA:dT)	Sigma	Cat#P0883-10UN
MCC950	AbMole Bioscience	Cat#M6164, CAS210826-40-7
Z-DEVD-FMK	Selleckchem	Cat#S7312
IM54	Cayman Chemical Company	Cat#13323
Necrostatin-1	AbMole Bioscience	Cat#M2315. CAS 4311-88-0
Ferrostatin-1	Adooq Bioscience	Cat#A13247, CAS 347174-05-4
Bafilomycin A1	abcam	Cat#ab120497
Allopurinol	Cayman Chemical Company	Cat# 10012597, CAS 315-30-0
Critical Commercial Assays		
Plasmid Mini Prep Kit	Jena Bioscience	PP-204L
Plasmid Midi Prep Kit	QIAGEN	12183
CytoTox-ONE Homogeneous Membrane Integrity Assay	Promega	G7890
Uric Acid/Uricase Assay kit	Cell Biolabs, inc.	STA-375
MitoSOX Red Mitochondrial Superoxide Indicator	Thermo Fisher Scientific	Cat#M36008
Human IL-1 beta/IL-1F2 DuoSet ELISA kit	R&D Biosystems	DY201
FuGENE® HD Transfection Reagent	Promega	E2311
Profect-P1-lipid based protein delivery reagent	Targeting Systems	#0041
Lipofectamine RNAiMAX Transfection Reagent	Thermo Fisher Scientific	13778075
Experimental Models: Cell Lines		
THP-1	ATCC	TIB-202
HEK293T	ATCC	CRL-11268
Hela229	ATCC	CCL-2.1

(*Continued on next page*)

Continued

REAGENT or RESOURCE	SOURCE	IDENTIFIER
THP-1 hGBP1 KO GFP	This paper	N/A
THP-1 hGBP1 KO +hGBP1 G68A	This paper	N/A
THP-1 hGBP1 KO +hGBP1 R48A	This paper	N/A
THP-1 hGBP1 KO +hGBP1 WT	This paper	N/A
THP-1 hGBP2 shRNA	Al-Zeer et al., 2013	N/A
Experimental Models: Organisms/Strains		
C. trachomatis, serovar L2	ATCC	VR-902B
Oligonucleotides		
SiRNA targeting sequence GDA #70	Thermo Fisher Scientific	Cat# 4392420, silencer select , s18470
SiRNA targeting sequence GDA #71	Thermo Fisher Scientific	Cat# 4392420, silencer select , s18471
SiRNA targeting sequence GDA #72	Thermo Fisher Scientific	Cat# 4392420, silencer select , s18472
siRNA targeting sequence CAS4 #1	Thermo Fisher Scientific	Cat#4390824, silencer select , s2413
siRNA targeting sequence CAS4 #2	Thermo Fisher Scientific	Cat#4390824, silencer select , s2414
hGBP1 KO Primer fw: CACCGACAAAGAGACGATAGCCCCC	This paper	N/A
GBP KO primer rv: AAACGGGGGCTATCGTCTCTTTGTC	This paper	N/A
qPCR primer actin fw: CAT GTA CGT TGC TAT CCA GGC	This paper	https://pga.mgh.harvard.edu/primerbank/
qPCR primer actin rv: CTC CTT AAT GTC ACG CAC GAT	This paper	https://pga.mgh.harvard.edu/primerbank/
qPCR primer GDA fw: TGA AGC CCA TAG TGA CAC CAC	This paper	https://pga.mgh.harvard.edu/primerbank/
qPCR primer GDA rv: GCA AAT CAC GGG TTT TAG CAA T	This paper	https://pga.mgh.harvard.edu/primerbank/
qPCR primer IL-1β fw: CAG GCT GCT CTG GGA TTC TC	This paper	https://pga.mgh.harvard.edu/primerbank/
qPCR primer IL-1β rv: CCT GGA AGG AGG AGC ACT TCA TCT	This paper	https://pga.mgh.harvard.edu/primerbank/
Recombinant DNA		
pSKB-LNB2-hGBP1	This paper	N/A
pSKB-LNB2-hGBP1 G68A	This paper	N/A
pSKB-LNB2-hGBP1 R48A	This paper	N/A
pSKB-LNB2-hGBP1 K76A	This paper	N/A
lentiCRISPR v2	Sanjana et al., 2014	Addgene #52961
plenti CMV GFP Hygro	Campeau et al., 2009	Addgene #17446
lentiCRISPR v2-hGBP1-KO	This paper	N/A
plenti CMV GFP Hygro hGBP1 WT	This paper	N/A
plenti CMV GFP Hygro hGBP1 R48A	This paper	N/A
plenti CMV GFP Hygro hGBP1 G68A	This paper	N/A
Software and Algorithms		
ImageJ	Schneider et al., 2012	https://imagej.nih.gov/ij/
Protein Calculator	N/A	http://protcalc.sourceforge.net/
Primer bank	Wang and Seed, 2003	https://pga.mgh.harvard.edu/primerbank/citation.html
UCSF Chimera	(Pettersen et al., 2004)	https://www.cgl.ucsf.edu/chimera/

RESOURCE AVAILABILITY

Lead Contact

Further information and requests for resources and reagents should be directed to and will be fulfilled by the Lead Contact, Oliver Daumke (oliver.daumke@mdc-berlin.de).

Materials Availability

All plasmids and cell lines generated in this study are available from the Lead Contact with a completed Materials Transfer Agreement.

Data and Code Availability

This study did not generate any unique datasets or code.

EXPERIMENTAL MODEL AND SUBJECT DETAILS

Cell Lines

THP-1 cell lines (American Type Culture Collection TIB-202) were cultured in RPMI 1640 with 10% fetal bovine serum (FBS). hGBP1 knock-out cell lines were generated by transfection of lentiCRISPRv2 containing hGBP1 single guide RNA sequences and single cell dilution. hGBP1 WT and mutant cell lines were generated by infection with lentiviruses generated in HEK293T cell line (ATCC CRL-11268) expressing hGBP1 proteins.

Human Primary Macrophages

Human primary macrophages were isolated from peripheral blood mononuclear cells (PBMCs) from healthy female donors, aged 20-40 years according to protocol number EA1/203/16 as approved by the ethics commission of Charité, Berlin. Human primary macrophages were cultured by adherence from PBMCs in RPMI 1640 with 10% FBS and 50 ng/ml human macrophage colony-stimulating factor (M-CSF) for 6 d.

Microbe strain and culture

C. trachomatis serovar L2 (ATCC VR-902B) was routinely, cultured, prepared, and propagated in HeLa cells (American Type Culture Collection CCL-2.1) as previously described (Al-Zeer et al., 2013).

METHOD DETAILS

Expression constructs

The hGBP1 mutants, R48A, K76A and G68A, were generated using the plasmid pQE80L-hGBP1 (a kind gift from Gerrit Praefcke) and the QuikChange site-directed mutagenesis kit (Stratagene, USA). The PCR product was cloned into a modified pET28 vector (pSKB-LNB2) and the mutation was verified by DNA sequencing.

Protein preparation

WT and mutant hGBP1 variants with an N-terminal His6 tag were expressed using pSKB-LNB2 in *E. coli* strain BL21(DE3). The cells were grown at 37°C in TB medium, and protein expression was induced at an optical density of 0.6-0.8 by the addition of 50 μM isopropyl-β-d-thiogalactopyranoside (IPTG), followed by overnight incubation at 18°C. Upon centrifugation, the cells were suspended in 50 mM Tris–HCl (pH 8.0), 5 mM $MgCl_2$, 500 mM NaCl, 5 mM β-mercaptoethanol, 10% (v/v) glycerol, 20 mM imidazole, 100 μM phenylmethylsulfonyl fluoride (PMSF) (Roth, Germany) and 1 μM DNase I (Roche) and mechanically lysed in a microfluidizer (Microfluidics). Following centrifugation (30,000 × g, 1 h, 4°C), the protein in the cleared lysate was applied to a NiNTA column (GE Healthcare) and eluted with 20 mM Tris–HCl (pH 8.0), 5 mM $MgCl_2$, 100 mM NaCl, 5 mM β-mercaptoethanol, 10% glycerol and 20 mM imidazole using a 20 mM to 500 mM imidazole gradient. It was followed by gel filtration via Superdex 200 (GE healthcare) in 50 mM HEPES pH 7.5, 5 mM $MgCl_2$ and 2 mM dithiothreitol. Fractions containing monomeric hGBP1 were pooled and concentrated using Amicon filters with a 10 kDa cut-off to 10 mg/ml, shock-frozen in liquid nitrogen and stored at −80°C. The concentration of hGBP1 was determined by ultraviolet spectrophotometry at 276 nm with the calculated molar absorption coefficient of 45,450 M^{-1} cm^{-1}.

GTP hydrolysis assay

Non-farnesylated hGBP1 WT and mutants at the indicated concentrations were incubated with 1 mM GTP at 37°C in buffer A (20 mM HEPES pH 7.5, 150 mM NaCl, 2 mM $MgCl_2$). Aliquots of the reaction were taken at the given time points, diluted in excess buffer A and flash-frozen in liquid nitrogen. Nucleotides were separated via reversed-phase chromatography (C-18, Hypersil) and their rations quantified by integration of the 260 nm absorbance.

Cell culture treatments and C. trachomatis infection

Human primary monocyte–derived macrophages (hMDMs) were prepared by adherence from whole-blood fractions of healthy donors. Primary monocytes were cultured in RPMI 1640 with 10% FBS and treated with 50 ng/mlM-CSF for 6 d. THP-1 cells were cultured in RPMI with 10% FCS. When indicated, THP-1 cells were differentiated with 100 nM phorbol 12-myristate 13-acetate (PMA) for 24 h. *C. trachomatis* bacteria were cultured as previously described (Al-Zeer et al., 2013) and infected at MOI 5 for inclusion count and infectivity assay, or at MOI 30 for inflammasome activation. For allopurinol specificity and inflammasome control experiments, THP-1 cells or hMDM were transfected either with 1 μg Flagellin (i.e., NLRC4 inflammasome stimulation) or 1 μg poly(dA:dT) (i.e., AIM2 inflammasome stimulation) for 6 h using Profect P1 reagent (Targeting Systems) or Lipofectamine RNAimax (Invitrogen), respectively. THP-1 cells or hMDMs were primed for 16 h with 100 nM LPS or 100 nM LPS + 100 nM IFN-γ, respectively, and treated with 5 mM ATP (NLRP3) for 4 h or transfected with 1 μg LPS (CAS4) for 6 h using FuGENE HD transfection reagent (Promega). For NLRP3 inhibition experiments, THP-1 cells or hMDMs were treated with 300 nM MCC950 for 1 h prior to 24 h infection with

C. trachomatis. For cell death pathway determination, THP-1 hGBP1 R48A mutant cells were treated with 12 μM IM-54, 1 μM Bafilomycin-A1, 40 μM necrostatin-1, 5 μM ferrostatin-1 or 15 μg/ml Ac-YVAD-CMK 1 h prior to 24 h infection with *C. trachomatis*. For the metabolite feedback experiments, THP-1 hGBP1 KO cells and THP-1 hGBP1 G68A mutant cells were treated with 0.5 mM or 1 mM guanine or guanosine for 1 h post infection (p.i.) with *C. trachomatis*.

CRISPR Cas9 mediated Knock out of hGBP1 in THP-1

hGBP1 single guide RNA sequences from Feng Zhang's Gecko database were cloned into lentiCRISPR v2 and transfected into THP-1 cells with Fugene HD transfection reagent (Promega). Two days after transfection, the cells were diluted into single clones and seeded into 96 well plates. Successful knockout of hGBP1 was confirmed via immunoblotting (rat anti hGBP1 1:1000, Santa Cruz biotechnology).

Immunostaining and ASC speck count

THP-1 cells were differentiated for 24 h with 100 nM PMA and infected with *C. trachomatis* at MOI 5 or 30 for 24 h. Cells were fixed in 4% Paraformaldehyde (PFA) or 2% PFA for a specific UA staining. After fixation, the cells were permeabilized with 0.3% Triton X-100 for 10 min and blocked in 3% bovine serum albumin (BSA) in phosphate-buffered saline or 10% horse serum, 100 mM glycine for 1 h at room temperature. The cells were stained for *C. trachomatis* inclusions (goat anti-MOMP 1:150), ASC (rabbit anti-ASC 1:300, Proteintech), Xanthine Oxidase (mouse anti XO, 1:50 Santa Cruz biotechnology), hGBP1 (rat anti hGBP1 1:50, Santa Cruz biotechnology), rabbit anti uric acid (UA, 1:1500), at 4°C, overnight. ASC specks were counted by evaluating 500 cells per experiment.

Inclusion count

THP-1 cells were differentiated with 100 nM PMA for 24 h and stimulated with 100 nM IFN-γ, 100 nM LPS for 24 h. The cells were infected with *C. trachomatis* at MOI 5. After 1 h of infection, the media was changed to fresh RPMI, and the cells incubated for another 23 h. The cells were fixed 24 h post infection (p.i.) with 4% PFA and stained for *C. trachomatis* and 4′,6-diamidino-2-phenylindole (DAPI). The number of inclusions per nuclei was determined following three independent experiments. In each experiment, 500 cells were evaluated. Significance was determined by one-way ANOVA.

Infectivity assay

Host cells were seeded in 6-well plates, treated as above, infected with *C. trachomatis* diluted in infectious medium at MOI 5 and incubated at 35°C and 5% CO_2. Two hours p.i., the cells were washed and loaded with fresh medium containing 100 U/ml IFN-γ. Control infected cells were not treated with the cytokine. The cell cultures were then incubated as above for 48 h. The formation of infectious *C. trachomatis* progeny in a secondary infection was assessed by infectivity titration assay (Al-Zeer et al., 2009). Briefly, the infected cells were mechanically destroyed using glass beads. Resulting lysates were serially diluted in infectious medium and then used to inoculate HeLa cells for 2 h. The cells were then washed and further incubated for 24 h in RPMI medium with 5% FBS and 1 μg/ml cycloheximide. One day later, the cells were fixed with 4% PFA and stained for *C. trachomatis*, as described above. Forty confocal images were taken per sample and experiment at 400x magnification, and the area of each image calculated and divided by the area of one well. The infectivity titer is expressed as the number of inclusions (IFU/ml) IFU/ml = no. inclusions in 10 fields/10 × no. fields in a well × dilution factor. Significance was determined by a Student's t test.

LDH cytotoxicity assay

THP-1 cells (1.7×10^5 per well) or hMDMs (2.0×10^5 per well) were stimulated with 100 nM IFN-γ and 100 nM LPS for 16 h and infected with *C. trachomatis* at MOI 30 for 24h in a 96-well plate or 24-well plate (hMDMs). LDH release upon infection was measured using CytoTox-ONE Homogeneous Membrane Integrity Assay kit (Promega, according to manufacturer's instructions). LDH release was calculated by subtraction of cell culture background and normalization to average maximum according to the Promega manual. Significance was determined by two-way ANOVA.

ELISA

THP-1 cells (1.7×10^5 per well) or hMDMs (2.0×10^5 per well) were stimulated with 100 nM IFN-γ and 100 nM LPS for 16 h and infected with *C. trachomatis* at MOI 30 for 24 h in a 96-well plate or 24-well plate (hMDMs). IL-1β measurements were conducted using the Human IL-1 beta/IL-1F2 DuoSet ELISA kit according to the manufacturer's instructions. Significance was determined by two-way ANOVA.

mtROS measurement

THP-1 cells (2×10^5 per well) were stimulated with 100 nM IFN-γ and 100 nM LPS for 16 h and infected with *C. trachomatis* at MOI 30 for 24 h in a 96-well plate. Mitochondrial ROS were measured by reaction with MitoSOX Red dye in a microplate reader according to manufacturer's instructions (fluorescence Ex.: 400nm/ Em.: 595 nm). Significance was determined by two-way ANOVA.

Uric acid measurement

THP-1 cells (2×10^5 per well) were stimulated with 100 nM IFN-γ and 100 nM LPS for 16 h and infected with *C. trachomatis* at MOI 30 for 24 h in a 96-well plate. Uric acid concentration in cell culture supernatants was measured using Uric acid/Uricase Assay Kit from Cell Biolabs, inc. according to the manufacturer's instructions. Briefly, uric acid reacts with water and oxygen in the presence of the enzyme uricase to produce allantoin and H_2O_2. In the presence of HRP, a fluorescence probe reacts with H_2O_2 in a 1:1 stoichiometry to produce a highly fluorescent product (Ex.: 535 nm/ Em.: 595 nm), which can be measured using a microplate reader.

QUANTIFICATION AND STATISTICAL ANALYSIS

Image Analysis

For inclusion and ASC speck counting approximately 30-40 images were taken per experiments representing approximately 500 cells. Nuclei, *C. trachomatis* inclusions and ASC specks were manually counted from immunostaining and analyzed statistically using one-way ANOVA in Graphpad Prism software. Infectivity titer was determined by counting *C. trachomatis* inclusions and nuclei from 40 images per sample and the area of each image calculated and divided by the area of one well. The infectivity titer is expressed as the number of inclusions (IFU/ml) IFU/ml = no. inclusions in 10 fields/10 × no. fields in a well × dilution factor. Significance was determined by Student's t test using Graphpad Prism software.

Cell Biological Assays

ELISA, LDH and mtROS assays were analyzed using two-way ANOVA and Uric acid measurements using one-way ANOVA in Graphpad Prism software for three independent experiments.

Cell Reports, Volume *31*

Supplemental Information

hGBP1 Coordinates *Chlamydia* Restriction and Inflammasome Activation through Sequential GTP Hydrolysis

Audrey Xavier, Munir A. Al-Zeer, Thomas F. Meyer, and Oliver Daumke

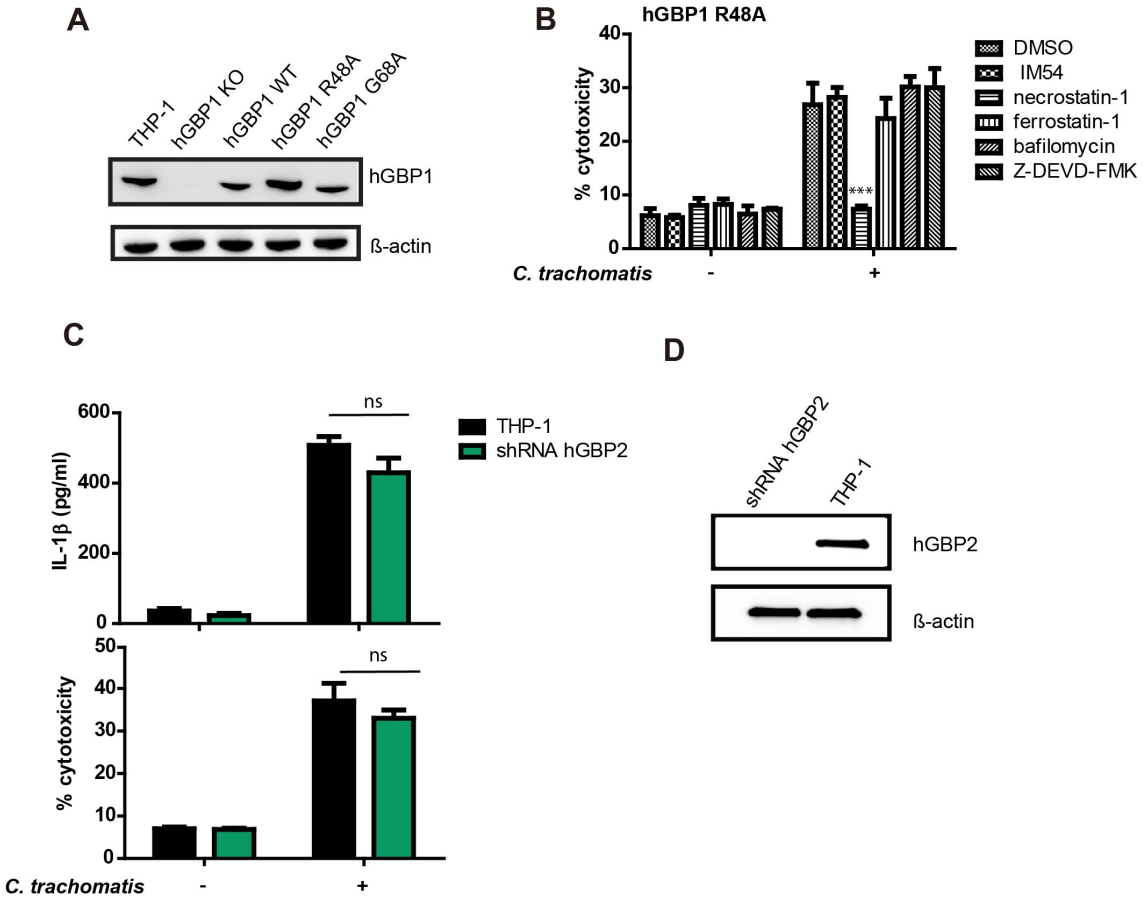

Figure S1. hGBP1 restricts *C. trachomatis*, related to Figure 2.

(A) CRISPR-Cas9-mediated knock-out of hGBP1 and stable overexpression of hydrolysis mutants as shown by immunoblotting. Cell lines were stimulated with IFN-γ for 16 h.

(B) LDH release of THP-1 hGBP1 R48A cell line stimulated with IFN-γ + LPS for 16 h, followed by infection with *C. trachomatis* at MOI 30 for 24 h. Cells were co-treated with indicated cell death inhibitors for 24 h, n=3; two-way ANOVA. Cell death inhibitors - IM54, necrostatin-1, ferrostatin-1, bafilomycin and Z-DEVD-FMK that inhibit necrosis, necroptosis, ferroptosis, autophagy and apoptosis, respectively.

(C) hGBP2 knock-down by shRNA in THP-1 cells. IL-1β ELISA and LDH release following infection with *C. trachomatis* at MOI 30 for 24 h, n=3; two-way ANOVA.

(D) Stable-knock down of hGBP2 in THP-1 cells shown by immunoblotting against hGBP2. Cells were treated with IFN-γ for 16 h.

All error bars indicate SEM. *P<0.05, **P<0.01, ***P<0.001.

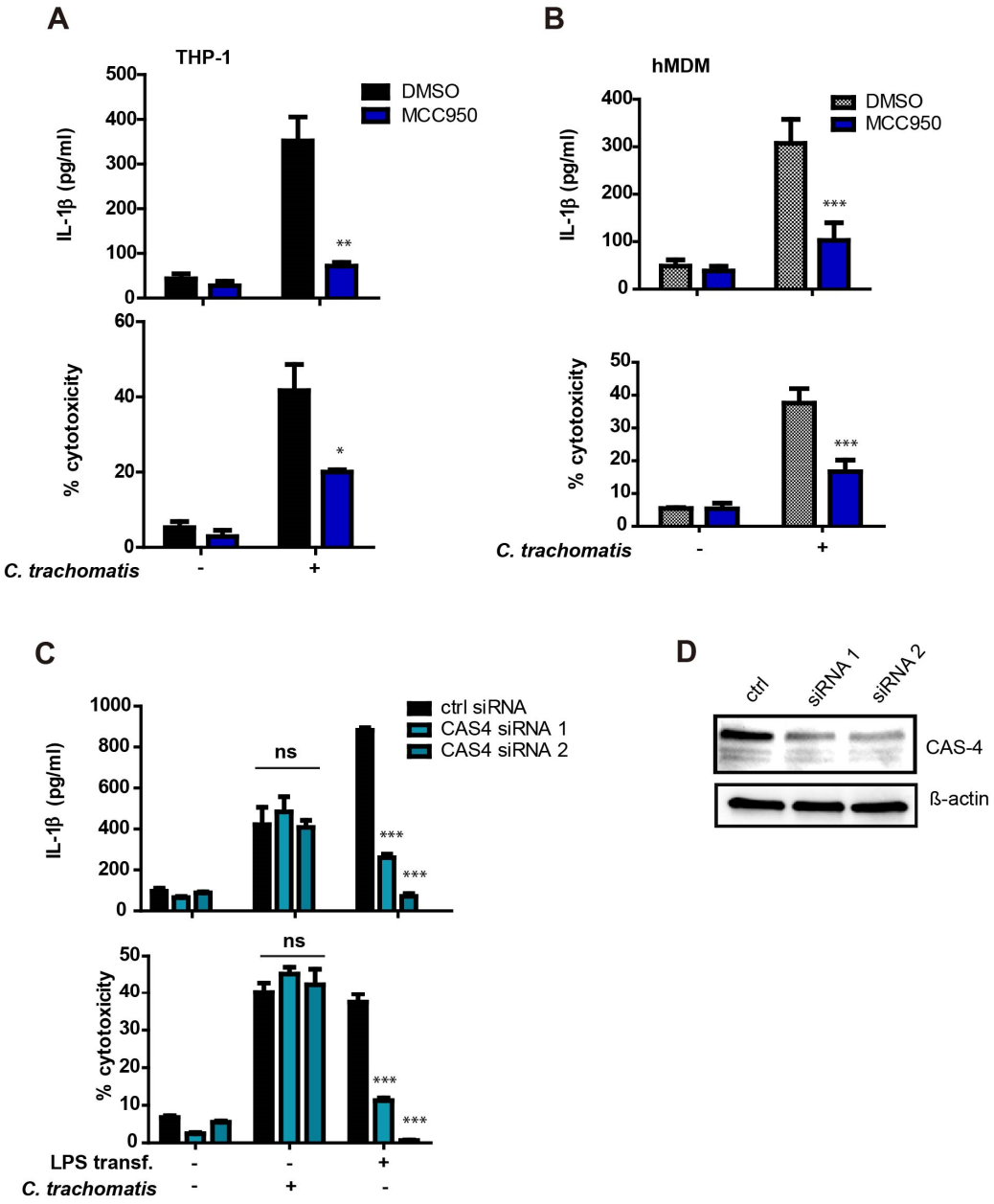

Figure S2. hGBP1 activates the caspase-4-independent NLRP3 inflammasome pathway upon *C. trachomatis* infection, related to Figure 3

(A) IL-1β ELISA and LDH release for THP-1 cells treated with MCC950 and infected with *C. trachomatis* at MOI 30 for 24 h, n=3; two-way ANOVA.

(B) IL-1β ELISA and LDH release for hMDMs treated with MCC950 and infected with *C. trachomatis* at MOI 30 for 24 h, n=3; two-way ANOVA.

(C) IL-1β ELISA and LDH release for THP-1 and THP-1 caspase-4 knock down cells, transfected with LPS or infected with *C. trachomatis* at MOI 30 for 24 h, n=3; two-way ANOVA.

(D) Transient knock down of caspase-4 in THP-1 cells was validated by immunoblotting against caspase-4. Cells were primed with IFN-γ and LPS.

*P<0.05, **P<0.01, ***P<0.001.

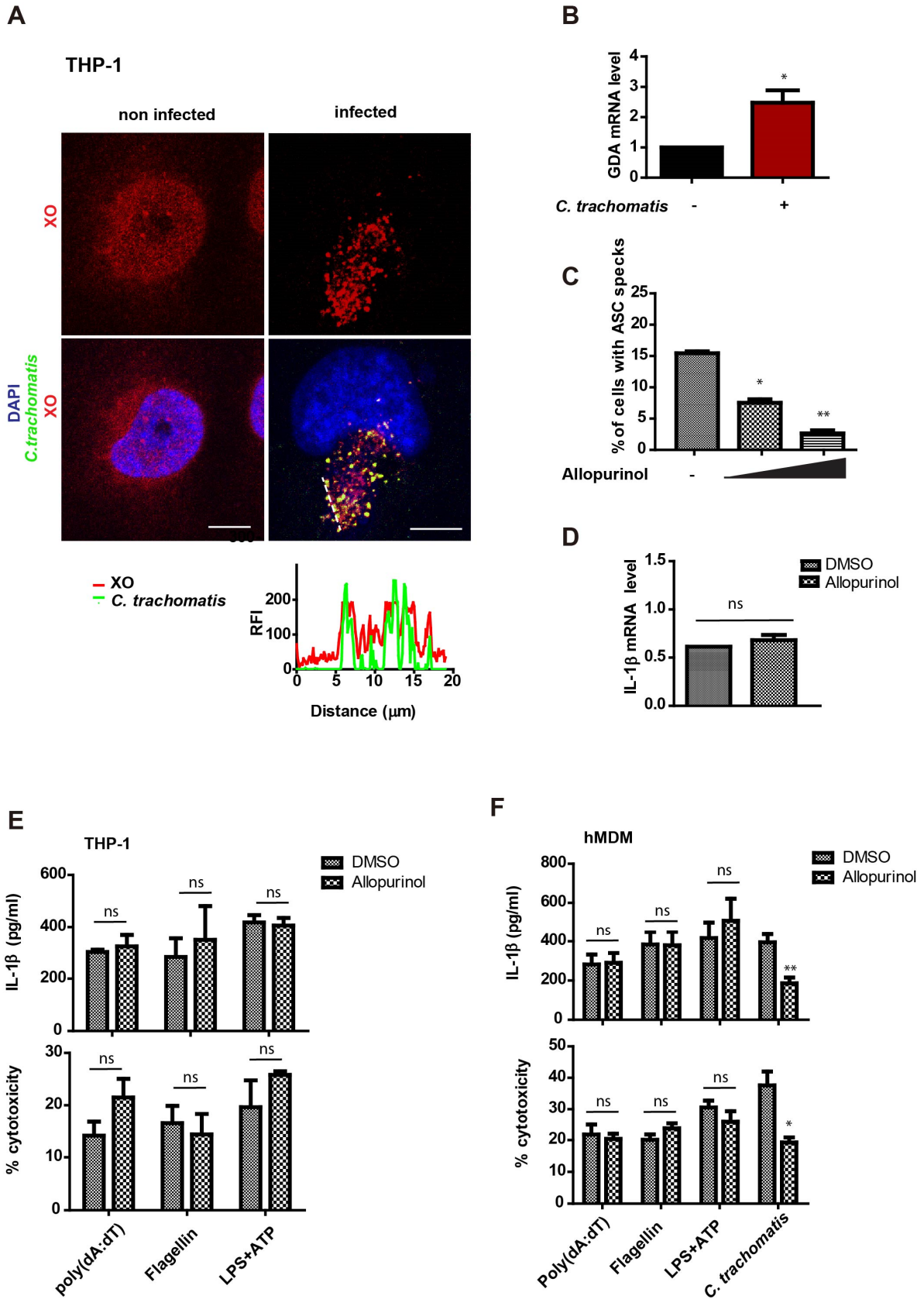
A
THP-1
non infected
infected
XO
DAPI
C.trachomatis
XO
XO
C. trachomatis
RFI
200
100
0
0 5 10 15 20
Distance (μm)
B
GDA mRNA level
4
3
2
1
0
*
C. trachomatis - +
C
% of cells with ASC specks
25
20
15
10
5
0
*
**
Allopurinol -
D
IL-1β mRNA level
1.5
1.0
0.5
0.0
ns
DMSO
Allopurinol
E
THP-1
DMSO
Allopurinol
IL-1β (pg/ml)
600
400
200
0
ns
ns
ns
% cytotoxicity
30
20
10
0
ns
ns
ns
poly(dA:dT)
Flagellin
LPS+ATP
F
hMDM
DMSO
Allopurinol
IL-1β (pg/ml)
800
600
400
200
0
ns
ns
ns
**
% cytotoxicity
50
40
30
20
10
0
ns
ns
ns
*
Poly(dA:dT)
Flagellin
LPS+ATP
C. trachomatis

Figure S3. Allopurinol specifically abrogates inflammasome activation upon *C. trachomatis* infection, related to Fig. 4.

(A) Representative images of xanthine oxidase (red) immunostaining with or without *C. trachomatis* (green) infection. The line tracing quantification of the white dashed line is shown at the bottom. Scale bar = 10 µm.

(B) mRNA levels of GDA in THP-1 cells upon infection or not with *C. trachomatis* at MOI 30 for 24 h, n=3; two-tailed Student´s t-test.

(C) Quantification of inflammasome ASC specks in THP-1 cells upon infection with *C. trachomatis* at MOI 30. The cells were co-treated with increasing concentrations of allopurinol (100 µM and 500 µM) for 24 h, n=3,; one-way ANOVA.

(D) mRNA levels of IL-1β in THP-1 stimulated and treated or untreated with allopurinol (500 µM), n=3; two-tailed Student´s t-test.

(E) IL-1β ELISA and LDH release of THP-1 cells, which were transfected with Flagellin, poly (dA:dT) or stimulated with LPS + ATP and co-treated with allopurinol (500 µM) as indicated, n=3; two-tailed Student´s t-test.

(F) IL-1β ELISA and LDH release of THP-1 cells transfected with Flagellin, poly (dA:dT) or stimulated with LPS + ATP or infected with *C. trachomatis* and co-treated with allopurinol (500 µM) as indicated, n=3; two-tailed Student´s t-test.

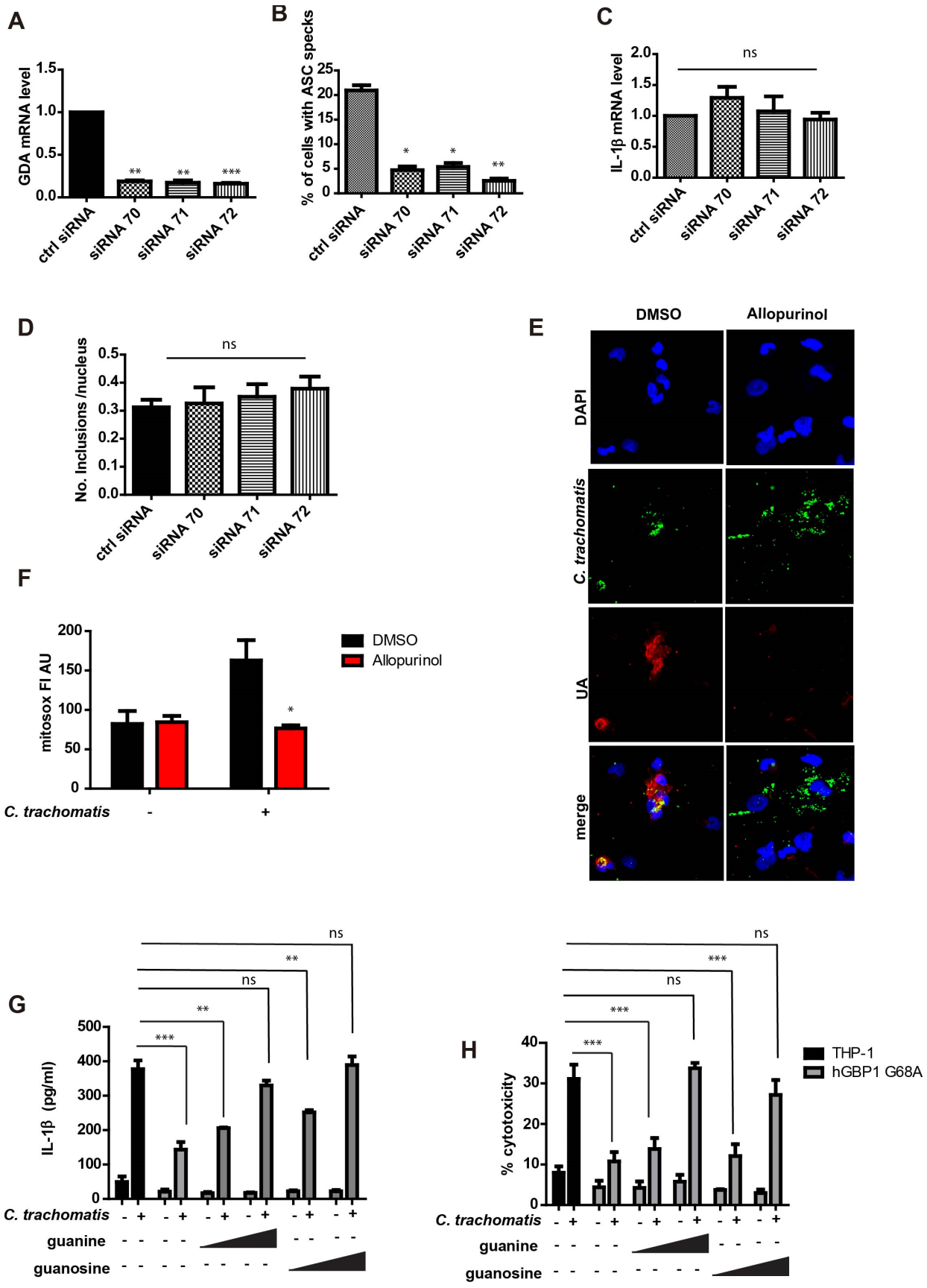
A
GDA mRNA level
1.5
1.0
0.5
0.0
**
**
***
ctrl siRNA
siRNA 70
siRNA 71
siRNA 72
B
% of cells with ASC specks
25
20
15
10
5
0
*
*
**
ctrl siRNA
siRNA 70
siRNA 71
siRNA 72
C
IL-1β mRNA level
2.0
1.5
1.0
0.5
0.0
ns
ctrl siRNA
siRNA 70
siRNA 71
siRNA 72
D
No. Inclusions /nucleus
0.5
0.4
0.3
0.2
0.1
0.0
ns
ctrl siRNA
siRNA 70
siRNA 71
siRNA 72
E
DMSO
Allopurinol
DAPI
C. trachomatis
UA
merge
F
mitosox FI AU
200
150
100
50
0
*
DMSO
Allopurinol
C. trachomatis - +
G
IL-1β (pg/ml)
500
400
300
200
100
0
ns
**
ns
**
***
C. trachomatis - + - + - + - + - + - +
guanine - - - - - - - -
guanosine - - - - - - - -
H
% cytotoxicity
40
30
20
10
0
ns
***
ns
***
***
THP-1
hGBP1 G68A
C. trachomatis - + - + - + - + - + - +
guanine - - - - - - - -
guanosine - - - - - - - -

Figure S4. Uric acid production upon *C. trachomatis* infection, related to Fig. 4.
(A) GDA knock down verification. GDA mRNA levels in THP-1 cells transfected with control or 3 different GDA siRNAs, n=3; one-way ANOVA.
(B) Quantification of inflammasome ASC specks in THP-1 transfected with 3 different GDA siRNAs, and infected with *C. trachomatis* at MOI 30 for 24 h, n=3; one-way ANOVA.
(C) mRNA levels of IL-1β in THP-1 cells transfected with three different GDA siRNAs (n=3; one-way ANOVA.
(D) Inclusion count of THP-1 cells transfected with three different GDA siRNAs and infected with *C. trachomatis* at MOI 5 for 24 h, n=3, one-way ANOVA.
Representative images of uric acid fluorescence intensity quantification, as in Fig. 4B.
(E) THP-1 cells were stimulated with IFN-γ + LPS, infected with *C. trachomatis* at MOI 30, and treated with allopurinol or DMSO. Cells were stained for *C. trachomatis* (green), uric acid (red) and DAPI (blue).
(F) Fluorescence intensity measurements of mitochondrial ROS in THP-1 cells infected or not with *C. trachomatis* and treated or not with 500 μM allopurinol, n=3; two-way ANOVA.
(G, H) IL-1β ELISA (G) and LDH release (H) of hGBP1 WT or G68A mutant cells infected with *C. trachomatis* at MOI 30 for 24 h and treated with increasing concentrations of guanine or guanosine (0.25 mM and 0.5 mM), n=3; significance was determined in comparison to the parental cells by two-way ANOVA.
All error bars indicate SEM. *P<0.05, **P<0.01, ***P<0.001.